



# Different approaches to obtain functionalized alumina as additive in polymer electrolyte membranes

Lucia Mazzapioda<sup>1</sup> · Mirko Sgambetterra<sup>1</sup> · Akiko Tsurumaki<sup>1</sup> · Maria Assunta Navarra<sup>1,2</sup>

Received: 6 April 2021 / Revised: 2 August 2021 / Accepted: 9 August 2021 / Published online: 10 September 2021  
© The Author(s) 2021

## Abstract

A series of sulfated aluminum oxides (S-Al<sub>2</sub>O<sub>3</sub>), investigated as an electrolyte additive in Nafion membranes, was synthesized *via* three different methods: (i) sol–gel sulfation starting from an aluminum alkoxide precursor, (ii) room temperature sulfation of fumed aluminum oxide, and (iii) hydrothermal sulfation of fumed aluminum oxide. Through the characterization of the synthesized S-Al<sub>2</sub>O<sub>3</sub> by means of X-ray diffraction (XRD), thermogravimetric analysis (TGA), and infrared (IR) spectroscopy, a higher sulfation rate was found to be achieved *via* a hydrothermal sulfation, and the coordination state of sulfate groups was identified as monodentate. By using this hydrothermally synthesized S-Al<sub>2</sub>O<sub>3</sub> as additive, a composite Nafion-based membrane was realized and compared to plain Nafion, by means of thermal analyses and fuel cell tests. Although higher hydration degree was found for the undoped membrane by differential scanning calorimetry (DSC), improved retention of fuel cell performance upon the increase of operation temperature was observed by using the composite electrolyte, confirming the stabilizing effect of the acidic inorganic additive.

**Keywords** Sulfated alumina · Nafion · Proton exchange membrane fuel cells

## Introduction

Polymer electrolyte membrane fuel cells (PEMFCs) are promising electrochemical devices with high energy conversion, high efficiency, and low environmental impact. The membrane electrode assembly (MEA) is the core component in PEMFC systems, which is composed of ion-exchange membrane coated with an electrode layer each side, where the electrochemical reactions take place, and this electrocatalytic layer is sandwiched by gas-diffusion layers [1, 2]. Although fuel cells are the promising energy conversion system, they are still not affordable and too expensive to be widely used as power generators. In particular, the most costly components in these devices are noble metal catalysts and perfluorinated membranes as electrolytes [3–5]. In order to be more competitive in the

field of renewable power sources, the cost of PEMFCs must be decreased. In addition, high performance durability and efficiency should be achieved at desired operating conditions which are high temperature ( $T > 80$  °C) and low relative humidity ( $RH < 30\%$ ). In these conditions, the electrode kinetics is enhanced and the cell overpotential is reduced, as well as the water management is facilitated compared to fully humidified devices [6].

The foremost famous benchmark material of proton exchange membrane is Nafion because of its high proton conductivity, good mechanical and electrochemical stabilities, and low permeability to fuels and electrons [7]. However, in PEMFCs operating at temperatures above 80 °C, Nafion membranes suffer from a severe decrease of proton conductivity because of water evaporation, resulting in a significant increase of the ohmic resistance [8, 9]. In addition, the Nafion polymer relaxation process, which occurs at around 80 °C, induces a shrinkage of the membrane and causes the degradation of electrolyte–electrode interface [10].

The addition of inorganic particles to the polymer membrane, and in particular of solid acids, is a promising strategy to develop composite electrolytes for high temperature fuel cells due to the ability of increasing the water retention

✉ Maria Assunta Navarra  
mariassunta.navarra@uniroma1.it

<sup>1</sup> Department of Chemistry, Sapienza University of Rome, Piazzale Aldo Moro 5, 00185 Rome, Italy

<sup>2</sup> CNR-ITAE, Istituto Di Tecnologie Avanzate Per L'Energia “Nicola Giordano”, Via Salita S. Lucia 5, 98126 Messina, Italy

capacity of the membrane, providing additional acid sites and also enhancing its thermal and mechanical properties [11, 12]. Conspicuous interest has been devoted to functionalized inorganic materials, including sulfated metal oxides (S-MO<sub>2</sub>), because of their dual property of high acidity and hygroscopicity which promote the water trapping in Nafion and create additional proton pathways through the membrane. This results in the enhancement of proton conductivity and improvement of the fuel cell performance at the desired conditions described above [13]. The morphology and the surface properties of these additives can be tuned to obtain nanometer sized particles as well as high and stable sulfation extent on the metal oxide. Furthermore, homogeneous dispersion of metal oxide particles in the Nafion matrix, to avoid phase segregation and fuel crossover through the membrane, is another aspect to be considered. Some sulfated particles based on zirconium [14, 15], titanium [16, 17], and tin [18] oxides have been investigated as additives in Nafion membranes for fuel cell devices, showing attractive results in terms of improved water affinity, enhanced proton conductivity, and mechanical features due to the presence of the inorganic particles within polymer matrix. Among all, sulfated aluminum oxide (S-Al<sub>2</sub>O<sub>3</sub>) is a very promising material for fuel cell applications because of its high intrinsic acidity and catalytic activity. Arata et al. successfully synthesized a super acidic sulfated alumina having the Hammett function scale ( $H_0$ ) ≤ 14.5 [19]. In our previous papers, we have investigated S-Al<sub>2</sub>O<sub>3</sub> to form hybrid composite membranes based on Nafion and demonstrated the positive influence of this inorganic filler on the temperature-dependent properties of the Nafion matrix [20]. However, there are no systematic studies about the particle synthesis procedure and sulfation degree, and therefore a strategy to obtain highly sulfated S-Al<sub>2</sub>O<sub>3</sub> has not yet been optimized. Also, during the synthesis procedure, the formation of undesired soluble ionic compounds, i.e., aluminum sulfate, should be controlled. Indeed, the presence of these impurities causes a decrease of stability of Nafion membrane under operating conditions of PEMFCs. To address these issues, herein, we report a

study on different synthesis approaches to produce pure S-Al<sub>2</sub>O<sub>3</sub> and emphasize its properties as additive in Nafion membranes.

## Experimental

### Synthesis of sulfated alumina oxides

As summarized in Table 1, six types of S-Al<sub>2</sub>O<sub>3</sub> were prepared by three different procedures. Sol-gel sulfated alumina (SGSA) was prepared as follows. Two grams of aluminum isopropoxide (≥ 98%, from Aldrich) was dispersed in 150 mL of 2-propanol and vigorously stirred for 2 h. Then, 50 mL of 0.5 M sulfuric acid was added and stirred for 0.5 h. The dispersion was filtered, dried, and calcined at 550 °C for 3 h (the temperature was increased at a rate of 3 °C min<sup>-1</sup> until 550 °C).

Sulfated fumed alumina (SFA) has been prepared via room temperature sulfation. A fumed aluminum oxide (≥ 99.8%, from Evonik Resource Efficiency GmbH) was primary calcinated at 550 °C for 3 h. The calcinated Al<sub>2</sub>O<sub>3</sub> was dispersed in a stirred H<sub>2</sub>SO<sub>4</sub> solution (3.2 M) for 1 h. The solid obtained was filtered and it was washed with distilled water several times until a neutral pH was reached. Finally, the sample was dried and calcinated at 550 °C for 3 h after an increase of 3 °C/min. In addition, to investigate the effect on sulfation of the initial calcination, the sample prepared without the thermal pretreatment was also investigated, which is called FSA-uc henceforth.

Hydrothermally sulfated fumed alumina (HSA) was prepared as follows. The fumed alumina was dispersed in 0.8 M H<sub>2</sub>SO<sub>4</sub> by stirring for 15 min and then autoclaved at 140 °C for 18 h. The precipitated solid was filtered and dried at 120 °C overnight. Finally, the obtained powders were calcinated at 550 °C for 3 h. The samples were also prepared without filtering and drying procedures, respectively, which are named HSA-uf and HSA-ud.

**Table 1** Preparation procedures and acronyms of the S-Al<sub>2</sub>O<sub>3</sub> samples

Procedure	Sol-gel sulfation		Room-T sulfation		Hydrothermal sulfation		
	SGSA		SFA	SFA-uc	HSA	HSA-uf	HSA-ud
Precursor	Aluminum isopropoxide		Fumed aluminum oxide		Fumed aluminum oxide		
Pretreatment of precursor	-		Calcination	-	-		
Sulfation condition	Mixed with 0.5 M H <sub>2</sub> SO <sub>4</sub> at r.t. for 0.5 h		Mixed in 3.2 M H <sub>2</sub> SO <sub>4</sub> at r.t. for 1 h		Autoclaved in 0.8 M H <sub>2</sub> SO <sub>4</sub> at 140 °C for 18 h		
Purification	Filtration and pre-dry		H <sub>2</sub> O rinsing and filtration		Filtration and pre-dry	Only pre-dry	Only filtration
Calcination	550 °C for 3 h		550 °C for 3 h		550 °C for 3 h		

## Membrane preparation

The solvents, which are used in commercially available Nafion dispersion (5 wt.% in water/alcohol, E.W. 1100, from Ion Power Inc), were gradually replaced with *N,N*-dimethylacetamide at 80 °C. For the preparation of composite membranes, S-Al<sub>2</sub>O<sub>3</sub> particles were added into the resulting solution. The filler concentration was adjusted to 5 wt.% with respect to the dry Nafion content, which was chosen as the optimal amount according to the literature [21, 22]. The solution obtained was casted in a Petri dish and dried at 100 °C. Dry membranes were hot-pressed at 175 °C, 50 atm for 15 min in order to improve the thermo-mechanical stability of the membranes. Finally, the samples were activated at 80 °C in the following solutions: 3% w/w hydrogen peroxide (H<sub>2</sub>O<sub>2</sub>, 34.5–36.5%, Sigma-Aldrich, St. Louis, MO, USA), sulfuric acid (0.5 M), and distilled water. A plain Nafion membrane was prepared by the same procedure and used as reference. All membrane samples were stored in distilled water.

## Chemical-physical characterizations

X-ray diffraction (XRD) analysis patterns on the inorganic compounds were collected using a Rigaku D-max Ultima + diffractometer equipped with a graphite monochromator in the  $2\theta$  range 10–90°. The K $\alpha$  radiation of Cu was used. The average crystallite size of S-Al<sub>2</sub>O<sub>3</sub> was calculated using the Debye–Scherrer equation ( $D = k\lambda/\beta\cos\theta$ ), in which  $k$  is a dimensionless shape factor, with a typical value of about 0.9 [23],  $D$  is the crystal size,  $\lambda$  is the wavelength of X-ray,  $\theta$  is the Bragg's angle in radians, and  $\beta$  is the full width at half maximum of the peak in radians.

Thermal analyses were conducted by means of thermal gravimetric analysis (TGA), using a TGA/SDTA851 (Mettler-Toledo, Zaventem, Belgium), as well as of differential scanning calorimetry (DSC), using a DSC821 instrument (Mettler-Toledo, Zaventem, Belgium). TGA was carried out from 25 to 900 °C in the case of S-Al<sub>2</sub>O<sub>3</sub> powder samples and from 100 to 600 °C in the case of dry membrane samples, under air flux at a scan rate of 5 °C min<sup>-1</sup>. DSC was carried out on fully humidified membrane samples in the temperature range between 100 and 180 °C at a scan rate of 20 °C min<sup>-1</sup> under nitrogen flux.

Fourier transform infrared (FTIR) spectroscopy measurements were performed on alumina powders by using a Bruker Alpha spectrometer in the frequency range 400–4000 cm<sup>-1</sup>. The S-Al<sub>2</sub>O<sub>3</sub> was dissolved in a KBr matrix and analyzed in transmission mode.

Fuel cell tests were performed by using a compact system (850C, Scribner Associates Inc, Southern Pines, NC, USA) connected to a 5 cm<sup>2</sup> cell fixture. The performances were analyzed in terms of cell potential, power density,

impedance spectroscopy, and the ohmic potential drop within the cell. The membrane electrode assembly (MEA) was prepared as follows: the surface of the electrodes (BASF, 0.5 mg Pt cm<sup>-2</sup>) was brushed with 0.4 mg Nafion solution, resulting in ca. 0.4 mg dry Nafion per cm<sup>-2</sup>. The membrane was hot-pressed between two electrodes at 120 °C and 10 atm for 7 min. The cell was fed with hydrogen and air under 1 atm at anode and cathode side, respectively. The humidification of the cell was accomplished by bubbling the fed gases through stainless steel cylinders incorporated in the compact system and containing distilled water. The temperature of the humidifiers, as well as that of the cell, was properly set to achieve the desired relative humidity. In operando electrochemical impedance spectroscopy (EIS) was performed with the 880 Impedance Analyzer in the 10 kHz–1 Hz frequency range. The amplitude of the sine wave was chosen to be 5% of the DC current present at 0.65-V cell potential. The impedance spectra were analyzed by the ZView software program (Scribner Associates) for the equivalent circuit fitting.

## Results and discussions

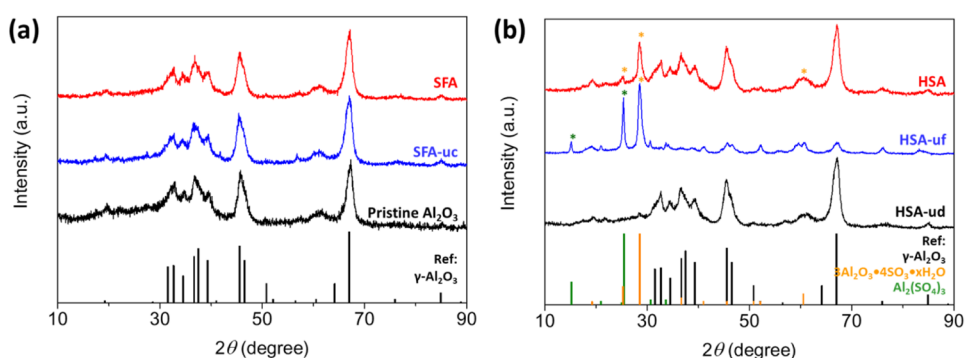
### Synthesis and structural analysis

The XRD patterns of S-Al<sub>2</sub>O<sub>3</sub> synthesized through the three different procedures are shown in Fig. 1 and S1. The presence of  $\gamma$ -alumina ( $\gamma$ -Al<sub>2</sub>O<sub>3</sub>, PDF#00–046–1131) phase has been confirmed in all the samples. In the case of SGSA (Figure S1), strong peaks assigned to aluminum sulfate (Al<sub>2</sub>(SO<sub>4</sub>)<sub>3</sub>, PDF#00–081–1835) were observed, which is an ionic compound not suitable for fuel cell application due to its solubility into water. Moreover, under fuel cell working conditions, such ionic species are expected to poison Nafion membrane conductivity, reducing the overall cell performance [24].

In the case of the series of SFA samples (Fig. 1(a)), only the peaks related to  $\gamma$ -Al<sub>2</sub>O<sub>3</sub> are visible. Therefore, the sulfated ratio of these samples is expected to be low. The crystallite size of these materials was calculated based on the most intense (4 0 0) peak at around 67°, and the values were very similar for all the samples (*i.e.*, 7.57, 7.57, and 7.37 nm for pristine Al<sub>2</sub>O<sub>3</sub>, SFA-uc, and SFA, respectively). The crystallite size of pristine Al<sub>2</sub>O<sub>3</sub> is preserved through this room temperature sulfation procedure. We therefore can confirm that this sulfation pathway is sufficiently mild, which does not cause the deterioration of pristine Al<sub>2</sub>O<sub>3</sub> crystalline structure, but not effective enough in terms of sulfation rate as the presence of sulfated alumina was not visible in the XRD spectra.

In contrast to the SGSA and SFA, the series of HSA samples exhibited multiple crystalline phases of  $\gamma$ -Al<sub>2</sub>O<sub>3</sub>,

**Fig. 1** X-ray diffraction pattern of S- $\text{Al}_2\text{O}_3$  synthesized via (a) room temperature sulfation and (b) hydrothermal sulfation. Bar charts denote the reference spectra of  $\gamma\text{-Al}_2\text{O}_3$  (PDF #00-046-1131),  $3\text{Al}_2\text{O}_3 \bullet 4\text{SO}_3 \bullet x\text{H}_2\text{O}$  (PDF # 00-016-0398), and  $\text{Al}_2(\text{SO}_4)_3$  (PDF # 00-081-1835)



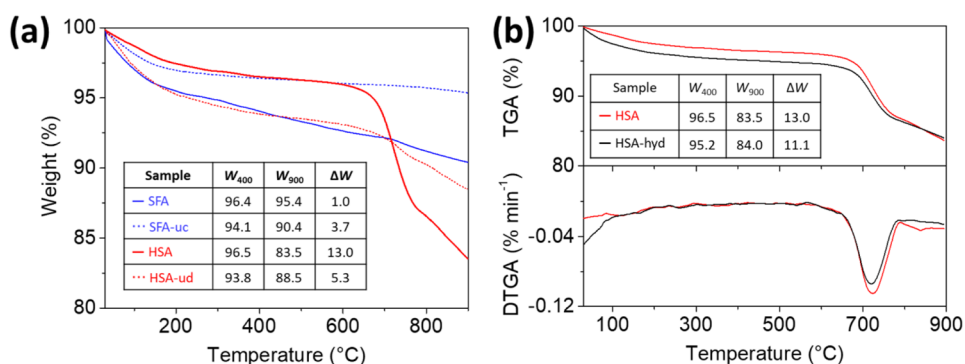
$3\text{Al}_2\text{O}_3 \bullet 4\text{SO}_3 \bullet x\text{H}_2\text{O}$ , and  $\text{Al}_2(\text{SO}_4)_3$  (Fig. 1(b)), and the composition of these materials was different depending on the purification procedures after the autoclave sulfation. The HSA-ud, which was not pre-dried prior to the calcination, exhibited solely the peaks of  $\gamma\text{-Al}_2\text{O}_3$ , while the HSA-uf, which was not filtered during the purification, showed intense peaks of  $\text{Al}_2(\text{SO}_4)_3$  and  $3\text{Al}_2\text{O}_3 \bullet 4\text{SO}_3 \bullet x\text{H}_2\text{O}$ , at  $15.1^\circ$ ,  $25.3^\circ$ , and  $28.5^\circ$ , and minor peaks associated to  $\gamma\text{-Al}_2\text{O}_3$ . The former result suggests that pre-drying at  $120^\circ\text{C}$  overnight before calcination is important to improve the sulfation ratio of aluminum oxide. However, when pre-drying was carried out without filtration, formation of  $\text{Al}_2(\text{SO}_4)_3$  was revealed, which is undesired for fuel cell applications. This is most likely because HSA-uf was dried in the presence of sulfate anion excess in the solution, since it was not filtered, and this can lead to the formation of ionic compounds. By combining the filtration and pre-dry procedures, HSA was obtained, and in this case, the peaks related to  $\gamma\text{-Al}_2\text{O}_3$  and  $3\text{Al}_2\text{O}_3 \bullet 4\text{SO}_3 \bullet x\text{H}_2\text{O}$  were observed. This means that both pretreatment procedures are necessary for the selective formation of  $3\text{Al}_2\text{O}_3 \bullet 4\text{SO}_3 \bullet x\text{H}_2\text{O}$  apart from  $\text{Al}_2(\text{SO}_4)_3$ . Because the presence of  $\text{Al}_2(\text{SO}_4)_3$  was confirmed in the case of SGSA and HSA-uf, these samples have been excluded from further assessments.

## Evaluation of sulfation ratio using TGA

In order to evaluate the amount of sulfate groups bonded to the aluminum oxide surface, TGA was performed on the four powder samples under air in a temperature range between  $25$  and  $900^\circ\text{C}$  (Fig. 2(a)). Below  $500^\circ\text{C}$ , the weight loss is generally derived from dehydration and removal of chemisorbed OH groups. S- $\text{Al}_2\text{O}_3$  samples are expected to show another important mass loss between  $500$  and  $900^\circ\text{C}$ , due to the removal of sulfate groups bonded to the surface of the alumina oxide.

In the table inserted in Fig. 2, the weight of samples at  $400^\circ\text{C}$  ( $W_{400}$ ) and  $900^\circ\text{C}$  ( $W_{900}$ ) and the difference between these values ( $\Delta W$ ) are reported. The  $\Delta W$  can be regarded as a sulfated ratio of S- $\text{Al}_2\text{O}_3$  in weight. The largest  $\Delta W$  was  $13.0\%$  for HSA, confirming a sufficient sulfation degree and suggesting a high surface acidity compared to the other samples. Especially, the SFA samples (blue curves) showed limited  $\Delta W$  less than  $4\%$ , which indicates that the room temperature synthesis does not promote the sulfation process effectively. In the case of HSA, the removal of sulfate groups from the sample occurred at the temperature above the calcination temperature, specifically  $550^\circ\text{C}$ , suggesting that the sulfate groups are strongly bonded to the oxide surface. In order to demonstrate this assumption, the HSA powder was

**Fig. 2** (a) TGA curves of the series of S- $\text{Al}_2\text{O}_3$  samples and (b) TGA-DTGA curves of HSA and hydrolized HSA (HSA-hyd) samples. The inset table summarizes the weight at  $400^\circ\text{C}$  ( $W_{400}$ ) and  $900^\circ\text{C}$  ( $W_{900}$ ), as well as the difference between them ( $\Delta W$ )





treated in boiling water and a new TGA trace was recorded (Fig. 2(b) HSA-hyd, top). The treated sample exhibits  $\Delta W$  of 11%, which is 2% smaller than that of pristine HSA. This is because some sulfate groups were lost due to the hydrolysis. However, major part of sulfate groups is present even after the harsh treatment, confirming a high stability of sulfate crystalline phase on the HSA surface. Furthermore, two types of sulfate groups differently bonded to the HSA sample surface become visible by performing derivative thermal gravimetric analysis (DTGA), as reported in Fig. 2(b), bottom. Specifically, two decomposition steps centered at ca. 723 °C and 836 °C are detected, the latter of which is diminished after the hydrolysis-stability test. As reported in literature [25], three different sulfate species, *i.e.* surface sulfate, multilayer sulfate, and crystallized  $\text{Al}_2(\text{SO}_4)_3$ , can be identified by the DTGA peaks at ca. 950 °C, 630 °C, and 800 °C, respectively. Similarly, in our case, the intense peak at the lower temperature is considered to arise from the sulfate groups organized in multilayers, whereas we deem the small and broad peak around 836 °C is attributed to the surface sulfate. Indeed, the presence of  $\text{Al}_2(\text{SO}_4)_3$  in HSA was not revealed by XRD analysis. In addition, according to the same literature, surface sulfate exhibits the peak centered at 950 °C, being it broad and starting below 800 °C when the  $\text{H}_2\text{SO}_4$  concentration of the sulfation solution is low alike the present study. After the hydrolysis, the peak around 836 °C was diminished which is probably because the surface sulfate groups were hydrolyzed and washed out during the treatment in boiling water. In contrast to the decrease in the peak intensity at 836 °C, the minor change of the peak at 726 °C confirms the high stability of sulfate groups organized in multilayers against the hydrolysis.

### FTIR results

With the aim of better interpretation about the sulfate coordination on  $\text{Al}_2\text{O}_3$ , FTIR spectroscopy measurements were carried out and reported in Fig. 3. The spectra of S- $\text{Al}_2\text{O}_3$  were compared to that of the pristine  $\text{Al}_2\text{O}_3$  powder as reference. In all the spectra, the distinctive bands related to Al-O bending vibrations were observed below 1000  $\text{cm}^{-1}$ . The spectra reported in Fig. 3 are therefore normalized by using the absorption intensity at 827  $\text{cm}^{-1}$ . In addition, the typical bands associated with the bending and stretching vibration of OH groups at 1630  $\text{cm}^{-1}$  and 3385  $\text{cm}^{-1}$  as well as the bands related to sulfate groups at around 1150  $\text{cm}^{-1}$  are observed. The intensity of the peak related to sulfate groups increased in the following order:  $\text{Al}_2\text{O}_3 < \text{SFA} < \text{SFA-uc} \sim \text{HSA-ud} < \text{HSA}$ , confirming the high sulfate concentration in the HSA sample.

The most important features for inorganic particles to be used as filler in Nafion composite membranes are its acidity and the adsorption property of water on its surface. In the

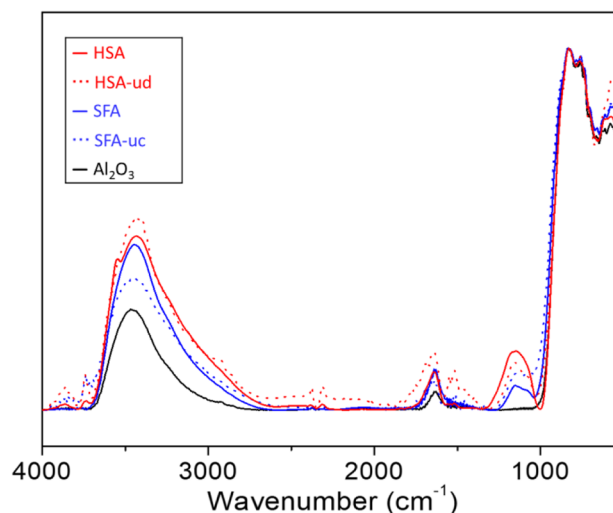
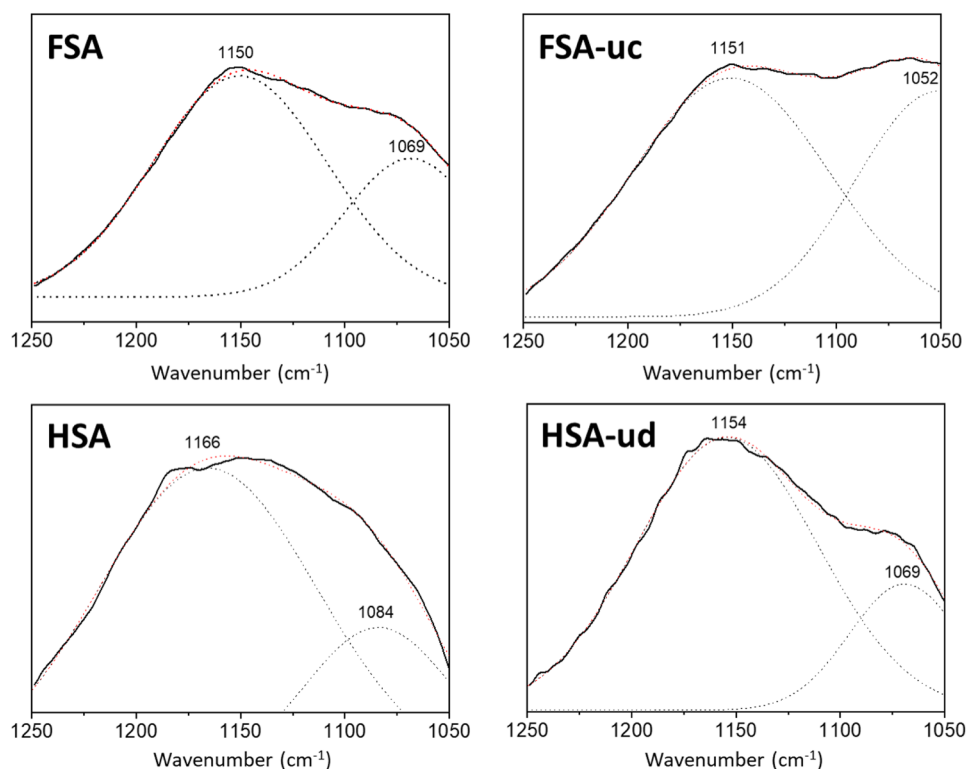


**Fig. 3** FTIR spectra of the series of SFA and HSA samples as well as the commercial alumina oxide

case of HSA sample, the O–H stretching vibration appearing at 3385  $\text{cm}^{-1}$  is broad and asymmetric. Aricò et al. [26] have reported that this broad peak can be divided into two: one in the range of 3040–3240  $\text{cm}^{-1}$  due to the surface acid–base functional O–H and the other in the range of 3400–3540  $\text{cm}^{-1}$  due to O–H of physically adsorbed water. Although the peak in the present study is difficult to decipher, taking similar positions and ratio of peak intensities into account, the main peak centered at 3385  $\text{cm}^{-1}$  is considered to be attributed to water physically adsorbed onto the oxide surfaces. In the same paper, it is also reported that this peak shifts to lower frequencies as a function of surface acidity of the filler, since the O–H bending frequency decreases due to strong hydrogen bonds of water with highly acidic fillers. In the present case, the peak position becomes lower in the following order:  $\text{Al}_2\text{O}_3$  (3460  $\text{cm}^{-1}$ ) > SFA-uc (3453  $\text{cm}^{-1}$ ) > SFA (3446  $\text{cm}^{-1}$ ) > HSA-ud and HSA (3433  $\text{cm}^{-1}$ ). Consequently, we assume that hydrothermally sulfated samples possess a higher acidity compared to SFA samples. To confirm this, the acidity of the sample was evaluated based on the ion-exchange capacity (IEC), which expresses the amount of exchangeable protons [27]. This analysis was performed by means of a titration method both for the HSA powder and for a plain  $\text{Al}_2\text{O}_3$ . The number of acid sites per gram was 0.15  $\text{meq g}^{-1}$  for  $\text{Al}_2\text{O}_3$  oxide and 0.35  $\text{meq g}^{-1}$  for the HSA sample. The superior surface acidity of HSA was thus confirmed.

Furthermore, the coordination mode of sulfate groups in S- $\text{Al}_2\text{O}_3$  can be recognized by analyzing the intense and asymmetric peak at about 1150  $\text{cm}^{-1}$  [28]. Upon the adsorption of sulfate onto mineral surfaces, the symmetry  $\nu_3$  band is known to split into either 3 or 2 peaks when bidentate

**Fig. 4** Gauss curve fitting of FTIR spectra of S-Al<sub>2</sub>O<sub>3</sub> samples



or monodentate coordination is formed, respectively [29]. As shown in Fig. 4, the asymmetric peak in the range of 1050–1250  $\text{cm}^{-1}$  can be accurately fitted by two Gaussian peaks in all cases, which suggests the formation of monodentate coordination of the sulfate groups on Al<sub>2</sub>O<sub>3</sub>. In the case of HSA, a visible deviation of the fitted curve (broken red line) from the original one (black solid line) was found at around 1170  $\text{cm}^{-1}$ . Even though the peak fitting using three Gaussian peaks did not converged, there is a possibility that HSA also includes bidentate sulfate groups. Interestingly, the linear correlation was found when the intensity ratio of the two peaks at higher frequency and lower frequency is plotted as a function of the sulfated ratio determined by means of TGA, *i.e.*  $\Delta W$  (Figure S2). Even though the change in peak intensity ratio has been frequently observed in similar systems, *i.e.* adsorption of sulfate onto several mineral compounds, the reason is still under discussion because the peak intensity can be caused by many factors such as adsorbed moisture and presence of free sulfate [30]. In the literature [31], the change in the peak intensity is explained by the possible formation of adsorbed bisulfate.

### Characterization of composite membranes

Composite membranes were then prepared by using HSA filler, which was filtrated and pre-dried prior to the calcination (see Table 1), that exhibited the most promising properties based on XRD, TGA, and FTIR analyses. The

obtained composite membrane samples, labelled as M-HSA, are opaque white, because of the presence of the inorganic additive particles, whereas plain Nafion membrane, used as reference for comparison purpose, is completely transparent. Each membrane results in uniform thickness, with values in the dry state of 85  $\mu\text{m}$  and 90  $\mu\text{m}$  for Nafion and M-HSA, respectively (Table 2).

The thermal stability of the membranes was investigated by TGA, reported in Figure S3. A slight weight loss below 300  $^{\circ}\text{C}$  is due to removal of water from the Nafion matrix [32]. A better thermal stability was found for pure Nafion, exhibiting higher decomposition temperature. The decomposition of Nafion occurs in three different steps [32]: (1) desulfonation process around 300  $^{\circ}\text{C}$ , (2) decomposition of perfluoroether side chains above 370  $^{\circ}\text{C}$ , and (3) decomposition of the fluorocarbon backbone above 430  $^{\circ}\text{C}$ . In the case of the composite membrane, the desulfonation was found to be comparable to that of pure Nafion membrane, while the decompositions of side chain and backbone occurred in a single step which was observed at lower temperature. This is

**Table 2** Properties of HSA-doped and undoped Nafion membranes

Acronym	Filler (%)	Thickness ( $\mu\text{m}$ )	$T_{\text{onset}}$ ( $^{\circ}\text{C}$ )	$\Delta H$ ( $\text{J g}^{-1}$ )
Nafion	0	85	131.2	454.8
M-HSA	5	90	142.8	248.0

known to occur when the Nafion matrix is rendered less mobile by the interaction with additives [33]. It is reported that the sulfated metal oxides have Lewis acid sites, which contribute to the formation of a Brønsted acid sites on the water molecule absorbed to the filler surface [15]. Similarly, in the present case, HSA filler itself has Lewis acid property, and the water absorbed on to the filler is expected to exhibit high hydrogen donor ability. Taking into consideration that Nafion has perfluorinated vinyl ether chains, Nafion is considered to form ion–dipole interactions with HSA and hydrogen bonds with the absorbed water. These interactions probably reduced the flexibility of Nafion matrix and caused the degradation phenomena at a lower temperature with respect to a pristine Nafion membrane. However, both membranes were confirmed to be stable in the temperature range, in which they are expected to be used as the electrolyte in PEMFCs [34].

Quantification of the state of water in the membrane is of great interest because it influences the proton transport properties of the membranes. Therefore, DSC analysis of M-HSA and Nafion was performed (Fig. 5), revealing that the endothermic peak attributed to order–disorder transition of ionic clusters in Nafion is present in both cases. The onset temperature ( $T_{\text{onset}}$ ) and the specific enthalpy value ( $\Delta H$ ) of the transition, calculated by the integration of the endothermic peak, are reported in Table 2. According to the literature [35], solely water interacting with hydrophilic Nafion matrix contributes to this thermal transition. In particular,  $\Delta H$  value increases by increasing the water content [20] because water is the major component in the ionic clusters, meanwhile the transition temperature decreases due to the plasticizer effect of water. As summarized in Table 2, the composite membrane shows a lower  $\Delta H$  value and a higher transition temperature compared to plain Nafion, suggesting

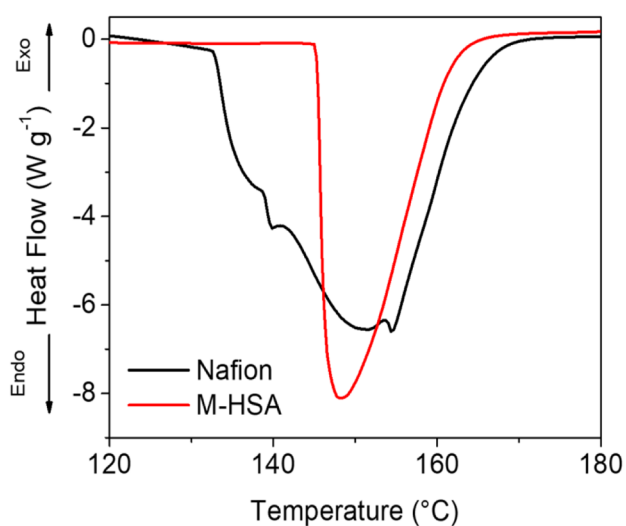


**Fig. 5** DSC curves of HSA-doped (red) and undoped Nafion membranes (black)

the hydration degree of M-HSA is lower than that of pristine Nafion. This finding can be explained as follows: it can be due to a non-optimized distribution of the filler within the Nafion matrix, which obstructs the mobility of the chain segments and restricts the release of water [36, 37], or it can be related to preferential filler-to-polymer interactions, preventing a direct coordination of water with the polymer hydrophilic groups. The latter is also supported by TGA results, where strong interactions of the acidic HSA filler with Nafion side chains were already supposed.

## Fuel cell performances

Fuel cell performances, employing the M-HSA composite membrane, were investigated as a function of temperature under humidified conditions. Figure 6 (a) shows polarization and power curves recorded at 70 °C and 90 °C. Results on an undoped Nafion-based fuel cell, investigated in the same conditions, are shown in Fig. 6 (b) as a reference, which

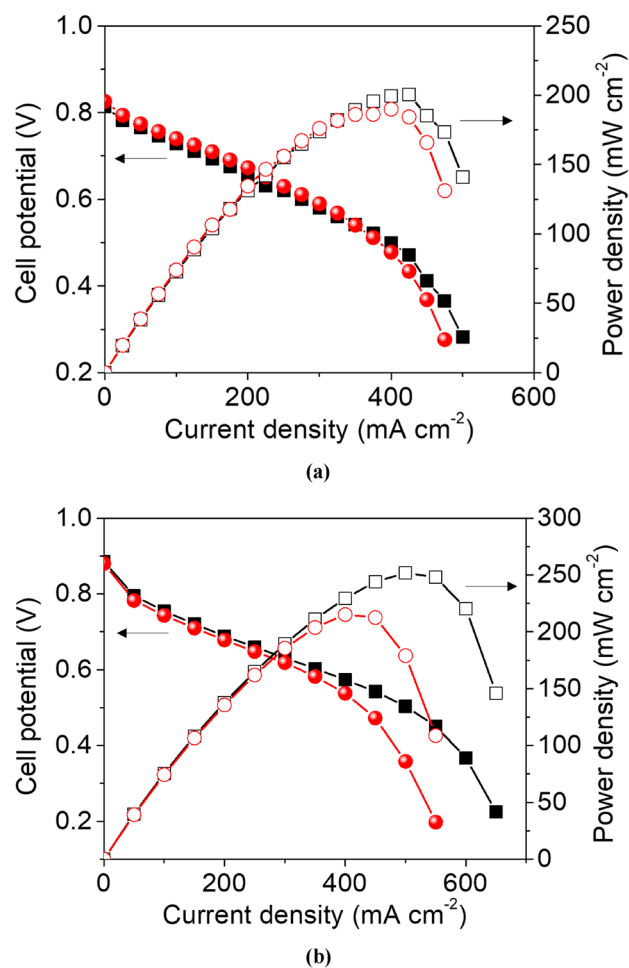
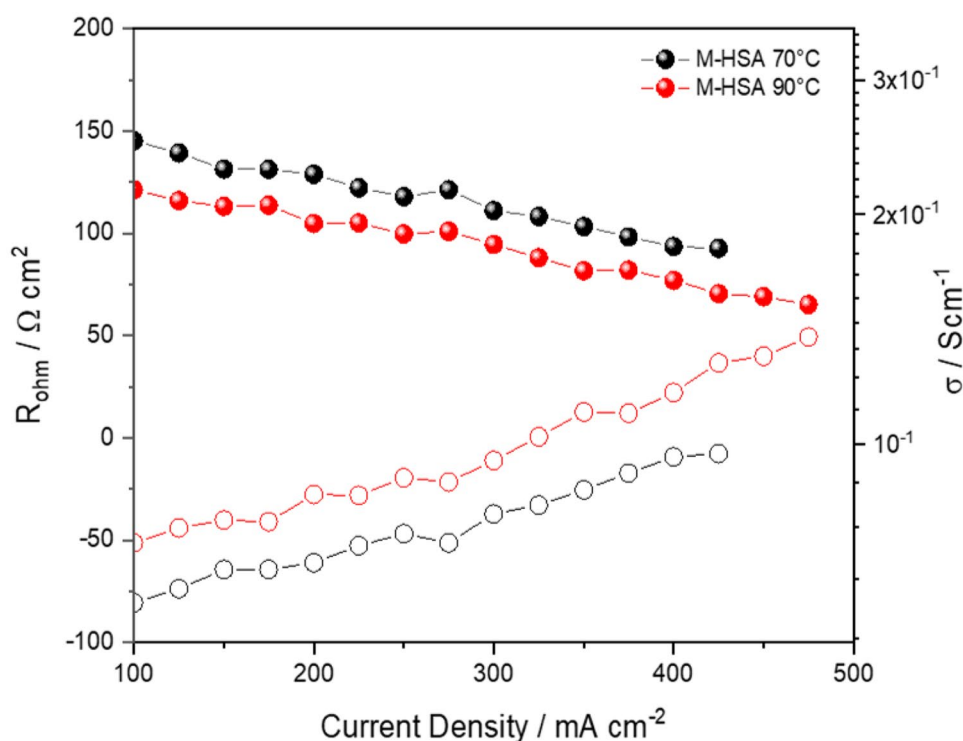


**Fig. 6** Comparison of PEMFC polarization and power density curves for the MEAs equipped with (a) the composite M-HSA and (b) pristine Nafion membrane at 70 °C (black) and 90 °C (red)

**Fig. 7** Ohmic ( $R_{\Omega}$ ) resistance (full symbols) and ionic conductivity (open symbols) values ( $\sigma$ ) during cell potential changes evaluated by the current interruption method



were already published in our previous work [20]. No performance improvements in terms of maximum current and power delivered are observed for the M-HSA-based system with respect to a plain Nafion membrane. In addition, the composite membrane shows a higher loss of potential, in particular in the activation and mass-diffusion regions of the polarization curve. As already discussed for the DSC analysis, a non-optimized distribution of HSA within Nafion matrix might be possible, hindering proton/water diffusivity and reducing the overall fuel cell performance.

The effect of our additive on the proton conduction resistance in the Nafion membrane was estimated by ohmic resistance measurements of the cell ( $R_{\text{ohm}}$  in  $\Omega \text{ cm}^2$ ) using the current interrupt method (Fig. 7). In our previous work [38], results on plain Nafion-based fuel cell, investigated in the same conditions for a membrane of comparable thickness, are published. The M-HSA composite membrane shows slightly higher  $R_{\text{ohm}}$  than plain Nafion membrane, suggesting a lower proton conductivity due to the presence of the inorganic

filler. However, the  $R_{\text{ohm}}$  of the cell decreases as the current density increases and reaches values lower than those of the plain Nafion membrane. Also, based on the value of  $R_{\text{ohm}}$ , the ionic conductivity was calculated and reported in Fig. 7 and Table 3. The conductivity is confirmed to be higher than  $10^{-2} \text{ S cm}^{-1}$  under the investigated conditions. It should be noted that this value is mainly related to the ionic conductivity of the membrane but it is also affected by the cell components and operating conditions because the ohmic and activation losses during cell potential changes are not separable [39, 40].

The ionic conductivity was also analyzed through in operando impedance spectroscopy, recorded while polarizing the cell at 0.65 V (Figure S4). In the ESI, the spectra of pristine Nafion are also reported as a reference. The spectra of the composite M-HSA were fitted by using the equivalent circuit  $R_{\Omega}(R_{\text{ct},1}Q)(R_{\text{ct},2}Q)$ , where  $R_{\Omega}$  is the ohmic resistance which corresponds to the intercept on the real axis in the higher frequency region,  $Q$  is the phase constant element, and  $R_{\text{ct},1}$  and  $R_{\text{ct},2}$  are the charge transfer resistances which reflect the

**Table 3**  $R_{\Omega}$  and  $R_{\text{ct}}$  evaluated by the current interrupt method at  $200 \text{ mA cm}^{-2}$  and EIS at 0.65 V, as well as  $\sigma$  calculated based on the  $R_{\Omega}$  values, for the composite M-HAS sample

Temperature (°C)	Current interrupt method @ $200 \text{ mA cm}^{-2}$		EIS @ 0.65 V				
	$R_{\Omega}$ (m $\Omega$ )	$\sigma$ (mS $\text{cm}^{-1}$ )	$R_{\Omega}$ (m $\Omega$ )	$R_{\text{ct},1}$ (m $\Omega$ )	$R_{\text{ct},2}$ (m $\Omega$ )	$R_{\text{ct}}^*$ (m $\Omega$ )	$\sigma$ (mS $\text{cm}^{-1}$ )
70 °C	25.7	69.9	24.1	117.2	64.4	181.6	74.7
90 °C	20.9	85.8	19.7	114.9	82.6	197.5	91.4

$$^*R_{\text{ct}} = R_{\text{ct},1} + R_{\text{ct},2}$$



diameter of semi-circles in the mid (200–10 Hz) and lower (10–1 Hz) frequency region, respectively. As summarized in Table 3, the  $R_{\Omega}$  and the corresponding ionic conductivity, evaluated by EIS, are comparable to those evaluated by the current interruption method under comparable polarization conditions (i.e., at 200 mA cm<sup>-2</sup>). As expected,  $R_{\Omega}$  decreases with temperature, due to lower activation energy towards proton conductivity in the membrane. By comparing these values, evaluated by EIS, with those of pristine Nafion membrane (Figure S4), it can be noticed that the HSA addition to the Nafion membrane does not compromise the ohmic resistance, and the unfavorable  $R_{ct}$  increase by the temperature rise is more controlled in the case of composite membrane. In the spectra of M-HSA, two overlapping semi-circles are visible in the mid-low frequency region, with the mid frequency arc due to the combination of an effective charge transference resistance for the oxygen reduction reaction (ORR) as well as double-layer capacitance within the catalyst layer, whereas the second arc at lower frequencies is associated with the mass-transport limitations of gas phase reactant within the gas diffusion media. In contrast to  $R_{\Omega}$  decreasing with temperature rise, the overall charge transfer resistance ( $R_{ct}$ ) increases with temperature, resulting in 181.6 m $\Omega$  at 70 °C and 197.5 m $\Omega$  at 90 °C, which is mainly caused by the increase of  $R_{ct,2}$ , i.e., the mass-transport resistance. Indeed, the cell potential plot below 0.5 V (see Fig. 6) decreases slightly more steeply at 90 °C. This behavior generally becomes more evident when fuel cell operates under fully humidified conditions because water can block micro pores in the catalyst layer and cause the mass-transport limitations in the O<sub>2</sub> diffusion layers [41].

It is worth noticing that a general good control in cell performance variation upon the temperature increase is obtained when using the composite M-HSA membrane. When the relative power density change ( $\Delta P$ ) is calculated, by considering maximum power density values, according to the following equation:

$$\Delta P(\%) = [(P_{90^{\circ}C} - P_{70^{\circ}C})/P_{90^{\circ}C}] * 100$$

the  $\Delta P$  values are found to be 8.7% for M-HSA and 17.2% for plain Nafion (called N cell in the literature [20]), which demonstrate that the M-HSA membrane is able to retain better performance at higher temperatures. Therefore, the addition of M-HSA was found to decrease the overall cell performance but to improve the temperature-dependent cell response.

## Conclusions

In the present work, the physical chemical properties of sulfated aluminum oxides, prepared by different synthetic routes and used as additive in Nafion membranes, are compared.

A tailored hydrothermal synthesis is proposed as the most convenient way, among those investigated, to obtain pure, super acidic S-Al<sub>2</sub>O<sub>3</sub>. Higher efficiency of sulfation was found in the following order: HSA > HSA-uf > FSA > FSA-uc, as confirmed by the presence of 3Al<sub>2</sub>O<sub>3</sub>•4SO<sub>3</sub>•xH<sub>2</sub>O in XRD analysis, the higher weight loss due to removal of sulfate groups in TG analysis, and a stronger peak intensity of the sulfate group in FTIR spectra. The Nafion membrane incorporating a 5 wt.% of HSA additive was investigated and its applicability in PEMFCs was tested. The M-HSA composite electrolyte showed lower hydration degree and fuel cell performances compared to plain Nafion, most likely due to a non-uniform dispersion of the filler and to preferential filler-to-polymer interactions, affecting water distribution. Anyhow, low ohmic resistance and better fuel cell performance retention are obtained by using M-HSA, with respect to undoped Nafion, when the cell operation temperature is increased. This highlights the beneficial effect of the acidic inorganic filler, supporting proton conductivity and stabilizing the membrane properties for higher temperature operation.

**Supplementary information** The online version contains supplementary material available at <https://doi.org/10.1007/s10008-021-05025-6>.

**Funding** Open access funding provided by Università degli Studi di Roma La Sapienza within the CRUI-CARE Agreement. The financial support of Sapienza University of Rome (Ateneo Call 2019, Project Number RM11916B863810FF) is gratefully acknowledged. ENEA, Agency for New Technologies, Energy and Sustainable Economic Development, is also acknowledged for the financial support within the PTR 2019–2021 “Accordo di Programma MiSE-ENEA *Sistema Elettrico Nazionale*”.

**Open Access** This article is licensed under a Creative Commons Attribution 4.0 International License, which permits use, sharing, adaptation, distribution and reproduction in any medium or format, as long as you give appropriate credit to the original author(s) and the source, provide a link to the Creative Commons licence, and indicate if changes were made. The images or other third party material in this article are included in the article's Creative Commons licence, unless indicated otherwise in a credit line to the material. If material is not included in the article's Creative Commons licence and your intended use is not permitted by statutory regulation or exceeds the permitted use, you will need to obtain permission directly from the copyright holder. To view a copy of this licence, visit <http://creativecommons.org/licenses/by/4.0/>.

## References

1. Rosli RE, Sulong AB, Daud WRW, Zulkifley MA, Husaini T, Rosli MI, Majlan EH, Haque MA (2017) A review of high-temperature proton exchange membrane fuel cell (HT-PEMFC) system. *Int J Hydrogen Energy* 42:9293–9314
2. Prykhodko Y, Fatyeyeva K, Hespel L, Marais S (2021) Progress in hybrid composite Nafion®-based membranes for proton exchange fuel cell application. *Chem Eng Technol* 409:127329–127344
3. Hernandez-Flores G, Poggi-Valardo HM, Solorza-Feria O (2016) Comparison of alternative membranes to replace high

- cost Nafion ones in microbial fuel cells *Int. J Hydrogen Energy* 41:23354–23362
- Hou J, Yang M, Ke C, Wei G, Priest C, Qiao Z, Wu G, Zhang J (2020) Platinum-group-metal catalysts for proton exchange membrane fuel cells: from catalyst design to electrode structure optimization. *EnergyChem* 2:100023–100032
  - Renzi M, Mignini P, Giuli G, Marassi R, Nobili F (2016) Rotating disk electrode study of Pt/Cs<sub>3</sub>HPMo<sub>11</sub>VO<sub>40</sub> composite catalysts for performing and durable PEM fuel cells. *Int J Hydrogen Energy* 41:11163–11173
  - Lizhong L, Bi H, Zongyi C, Qifei J (2020) Improved water management by alternating air flow directions in a proton exchange membrane fuel cell stack. *J Power Sources* 466:228311–228324
  - Siracusano S, Oldani C, Navarra MA, Tonella S, Mazzapioda L, Briguglio N, Aricò AS (2019) Chemically stabilised extruded and recast short side chain Aquivion® proton exchange membranes for high current density operation in water electrolysis. *J Membr Sci* 578:136–148
  - Owejan JP, Gagliardo JJ, Sergi JM, Kandlikar SG, Trabold TA (2009) Water management studies in PEM fuel cells. Part I. Fuel cell design and in situ water distributions. *Int J Hydrogen Energy* 34:3436–3444
  - Rossi Albertini V, Paci B, Nobili F, Marassi R, Di Michiel M (2009) Time/space-resolved studies of the Nafion membrane hydration profile in a running fuel cell. *Adv Mater* 21:578–583
  - Teocoli F, Paolone A, Palumbo O, Navarra MA, Casciola M, Donnadio A (2012) Effects of water freezing on the mechanical properties of Nafion membranes. *J Polym Sci Pol Phys* 50:1421–1425
  - Nicotera I, Kosma V, Simari C, Ranieri GA, Sgambetterra M, Panero S, Navarra MA (2015) An NMR study on the molecular dynamic and exchange effects in composite Nafion/sulfated titania membranes for PEMFCs. *Int J Hydrog Energy* 40:14651–14660
  - Liu B, Hu Bo DuJ, Cheng D, Zang H-Y, Ge X, Tan H, Wang Y, Duan X, Jin Z, Zhang W, Li Y, Su Z (2021) Precise molecular-level modification of Nafion with bismuth oxide clusters for high-performance proton-exchange membranes *Angew. Chem* 133:6141–6150
  - Sgambetterra M, Panero S, Hassoun J, Navarra MA (2013) Hybrid membranes based on sulfated titania nanoparticles as low cost proton conductors. *Ionics* 19:1203–1206
  - Siracusano S, Baglio V, Navarra MA, Panero S, Antonucci V, Aricò AS (2012) Investigation of composite Nafion/sulfated zirconia membrane for solid polymer electrolyte electrolyzer applications. *Int J Electrochem Sci* 7:1532–1542
  - Hara S, Miyama M (2004) Proton conductivity of superacidic sulfated zirconia. *Sol State Ionics* 168:111–116
  - Allodi V, Brutti S, Giarola M, Sgambetterra M, Navarra MA, Panero S, Mariotto G (2016) Structural and spectroscopic characterization of a nanosized sulfated TiO<sub>2</sub> filler and of nanocomposite Nafion membranes. *Polymers* 8:68–81
  - Siracusano S, Baglio V, Nicotera I, Mazzapioda L, Aricò AS, Panero S, Navarra MA (2017) Sulfated titania as additive in Nafion membranes for water electrolysis applications. *Int J Hydrog Energy* 42:27851–27858
  - Brutti S, Scipioni R, Navarra MA, Panero S, Allodi V, Giarola M, Mariotto G (2014) SnO<sub>2</sub>-Nafion® nano composite polymer electrolytes for fuel cell applications. *Int J Nanotechnol* 11:882–896
  - Arata K (2009) Organic syntheses catalyzed by superacidic metal oxides: sulfated zirconia and related compounds. *Green Chem* 11:1719–1728
  - Branchi M, Sgambetterra M, Pettiti I, Panero S, Navarra MA (2015) Functionalized Al<sub>2</sub>O<sub>3</sub> particles as additives in proton-conducting polymer electrolyte membranes for fuel cell applications. *Int J Hydrog Energy* 40:14757–14767
  - Chen F, Mecheri B, D'Epifanio A, Traversa E, Licocchia S (2010) Development of Nafion/tin oxide composite MEA for DMFC applications. *Fuel Cells* 5:790–797
  - Mazzapioda L, Lo Vecchio C, Danyliv O, Baglio V, Martinelli A, Navarra MA (2020) Composite Nafion-CaTiO<sub>3-δ</sub> membranes as electrolyte component for PEM fuel cells. *Polymers* 12:2019–2023
  - Holzwarth U, Gibson N (2011) The Scherrer equation versus the 'Debye-Scherrer equation.' *Nature Nanotech* 6:534
  - Hongsirikarna K, Goodwin JG Jr, Greenway S, Creager S (2010) Influence of ammonia on the conductivity of Nafion membranes. *J Power Sources* 195:30–38
  - Yang T, Chang T, Yeh C (1997) Acidities of sulfate species formed on a superacid of sulfated alumina. *J Mol Catal A: Chem* 115:339–346
  - Aricò AS, Baglio V, Di Blasi A, Creti P, Antonucci PL, Antonucci V (2003) Influence of the acid-base characteristics of inorganic fillers on the high temperature performance of composite membranes in direct methanol fuel cells. *Electrochem Commun* 5:862
  - Neelakandan S, Kanagaraj P, Nagendran A, Rana D, Matsuura T, Muthumeenal A (2015) Enhancing proton conduction of sulfonated poly (phenylene ether ether sulfone) membrane by charged surface modifying macromolecules for H<sub>2</sub>/O<sub>2</sub> fuel cells. *Renew Energy* 78:306–313
  - Infrared NK, Raman spectra of inorganic and coordination compounds. (1992) Part A. John Wiley & Sons 1992:248–250
  - Hug JS (1997) In situ Fourier transform infrared measurements of sulfate adsorption on hematite in aqueous solutions. *J Colloid Interf Sci* 188:415–422
  - Mendez JC, Tjisse HT (2018) Carbonate adsorption to ferrihydrite: competitive interaction with phosphate for use in soil systems. *ACS Earth Space Chem* 2:387–398
  - Paul KW, Borda MJ, Kubicki JD, Sparks DL (2005) Effect of dehydration on sulfate coordination and speciation at the Fe(hydr) oxide–water interface: a molecular orbital/density functional theory and Fourier transform infrared spectroscopic investigation. *Langmuir* 21:11071–11078
  - Adjemian KT, Dominey R, Krishnan L, Ota H, Majsztrik P, Zhang T, Mann J, Kirby B, Gatto L, Velo-Simpson M, Leahy J, Srinivasan S, Benziger JB, Bocarsly AB (2006) Function and characterization of metal oxide Nafion composite membranes for elevated-temperature H<sub>2</sub>/O<sub>2</sub> PEM fuel cells. *Chem Mater* 18:2238–2248
  - Deng Q, Wilkie CA, Moore RB, Mauritz, (1998) TGA-FTi.r. investigation of the thermal degradation of Nafion® and Nafion®/[silicon oxide]-based nanocomposites. *Polymer* 39:5961–5972
  - Mazzapioda L, Navarra MA, Trequattrini F, Paolone A, Elamin K, Martinelli A, Palumbo O (2019) Composite Nafion membranes with CaTiO<sub>3-δ</sub> additive for possible applications in electrochemical devices. *Membranes* 9:143–155
  - Lage LG, Delgado PG, Kawano Y (2004) Thermal stability and decomposition of Nafion® membranes with different cations. *J Therm Anal Calorim* 75:521–530
  - Mazzapioda L, Panero S, Navarra MA (2019) Polymer electrolyte membranes based on Nafion and a superacidic inorganic additive for fuel cell applications. *Polymers* 11:914–924
  - Sgambetterra M, Brutti S, Allodi V, Mariotto G, Panero S, Navarra MA (2016) Critical filler concentration in sulfated titania-added Nafion<sup>TM</sup> membranes for fuel cell applications. *Energies* 9:272–287
  - Navarra MA, Abbati C, Croce F, Scrosati B (2009) Temperature-dependent performances of a fuel cell using a superacid zirconia doped Nafion polymer electrolyte. *Fuel Cells* 3:222–225
  - Radev I, Georgiev G, Sinigersky V, Slavcheva E (2008) Proton conductivity measurements of PEM performed in Easy Test Cell. *Int J Hydrog Energy* 33:4849–4855

40. Abe T, Shima H, Watanabe K, Ito Y (2004) Study of PEFCs by AC impedance, current interrupt, and dew point measurements. *J Electrochem Soc* 151:A101–A105
41. Araya SS, Zhou F, Sahlin SL, Sobi T, Jeppesen C, Knudsen S (2019) Fault characterization of a proton exchange membrane fuel cell stack. *Energies* 12:152–169